Check for updates

Evolution of self-healing performance of UHPC exposed to aggressive environments and cracking/healing cycles

Bin Xi · Liberato Ferrara

Abstract This paper investigates the resilience of UHPC's self-healing capabilities under aggressive environmental conditions and cracking/healing cycles. UHPC specimens 'with a double-edged wedge splitting geometry were made, incorporating a commercial crystalline admixture (Penetron Admix®). The evaluation of UHPC's healing capacity involved subjecting pre-cracked samples to three different water immersion conditions: tap water, saltwater, and geothermal water. The closure of cracks during different curing periods was meticulously recorded using optical microscopy. Furthermore, specialized tests, including ultrasonic pulse velocity (UPV) measurements and splitting tensile tests, were conducted to quantify the recovery of mechanical properties. The results reveal that extended exposure results in a gradual closure of cracks, where salt water and geothermal water exhibit lower self-healing capabilities. Self-healing improves after the 1st crack/self-healing cycle but decline rapidly after the 2nd cycle. Mechanical property is strongly correlated with the extent of self-healing, and all samples display varying degrees of stiffness recovery, with the most pronounced recovery occurring after the 1st cycle. However, following the 2nd cycle, the stiffness recovery values decrease due to repeated loading, resulting in increased damage and a reduced number of reactive particles, thereby compromising self-healing and stiffness recovery. Despite enduring multiple instances of crack damage, UHPC samples still exhibit notable toughness recovery, underscoring the enduring efficacy of the self-healing mechanism even in challenging conditions.

Keywords UHPC · Durability · Self-healing · Aggressive environments

1 Introduction

Concrete and concrete structures have seen significant changes and undergone challenging developments in the last decades, focusing on improving material and structural performance, safety, and reliability, while also embracing sustainability principles [1]. This shift places stricter demands on material properties and the need to reduce material use and maintenance costs for structures. With advancing technology, dedicated researchers and engineers have been continuously exploring new material concepts and design approaches to enhance the multifold set of performance required to satisfy the requirements of safety, serviceability, durability and sustainability [2]. Additionally, efforts are made to provide concrete properties that help it to better withstand mechanical and

B. Xi · L. Ferrara (✉)
Department of Civil and Environmental Engineering,
Politecnico di Milano, Milan, Italy
e-mail: liberato.ferrara@polimi.it

B. Xi
e-mail: bin.xi@polimi.it

environmental stresses, reducing the impact of aging and material deterioration [3, 4].

Ultra-High Performance Concrete (UHPC) has gained significant attention due to its outstanding mechanical strength and durability, leading to rapid growth and widespread use in recent years [5–8]. Impressively, UHPC does not only achieve a compressive strength of over 150 MPa after 28 days, and by the introduction of steel fibres, the material achieves strain-hardening behaviour in the tensile state [9]. This helps to effectively control the spread of cracks, distributing the damage, otherwise localized into a single major crack, into a set of tightly spaced, thinly opened and stably propagating microcracks, each measuring only 0.02–0.03 mm in width [10] which also allows UHPC to reach ultimate strains even higher than the conventional'steel reinforcement yield strain (0.2%) while being able to continuing sustaining a not negligible tensile stress [11, 12]. These remarkable properties make UHPC a top choice for structures requiring superior mechanical strength and long-term durability, including, e.g. bridges, wind towers and tunnels [13–15].

However, concrete cracking is an inevitable occurrence, even in UHPC structures. There are various factors leading to cracking such as mechanical loads, fluctuations in temperature and humidity, restrained shrinkage, creep deformation, and environmental actions, including chemical attacks. When UHPC that is already cracked is exposed to harsh environmental conditions, detrimental ions from the surroundings can infiltrate through these cracks, targeting the cement matrix and the fibre reinforcement within the UHPC structure. This infiltration, and the ensuing degradation processes, could lead to significant deterioration in the properties of the UHPC.

Fortunately, the concept of self-healing techniques offers a promising solution to address the cracking issue. Previous studies have already demonstrated that the utilization of effective self-healing materials can significantly enhance the durability of structures while minimizing maintenance costs [4, 16]. UHPC possesses inherent qualities that support crack sealing, thanks to the ongoing hydration reaction of cement particles and the carbonation of hydration products [17, 18], fostered by the mix-design composition which, featuring high binder content and low water/binder ratio, leaves large amount of potentially reactive un-hydrated binder particles in the bulk of the "in-structure" material. Additionally, researchers have made significant progress in enhancing UHPC's self-healing abilities through various approaches. These methods include adjusting the type and quantity of supplementary cementitious materials (SCMs), incorporating crystalline admixtures (CAs) [19], and utilizing autonomous self-healing methods including encapsulated polymer healing agents [20], swelling agents like Super Absorbent Polymers (SAP) [21], and capsules containing bacteria [22]. These advancements hold great potential for improving the long-term durability and performance of UHPC structures, addressing concerns related to crack formation and material performance degradation.

The repeatability of self-healing materials' performance holds significant importance as it serves as a crucial indicator of structural stability. Snoeck and De Belie [23] conducted an investigation to assess the capacity of Strain-Hardening Cementitious Composites (SHCC) to consistently induce autogenous healing following two loading cycles within a four-point bending test. In this study, SHCC beams were initially pre-cracked and subjected to strain limitations of up to 1%. Subsequently, after an additional 28-day healing period, the specimens underwent a second round of loading and failure test occurred during the third loading cycle. During wet and dry cycles, SHCC specimens without superabsorbent polymers (SAPs) demonstrated a recovery rate of 46% of their initial crack strength after the first healing cycle. This recovery rate decreased to 28% after the second healing cycle. SHCC beams incorporating SAPs exhibited significantly enhanced recovery rates. Specifically, they achieved a recovery rate of 75% after the first healing cycle and maintained a recovery rate of 66% after the second healing cycle. Cuenca et al. [24] conducted an analysis focused on evaluating the self-healing capacity of steel fibre concrete in the presence and absence of crystalline admixtures, particularly under conditions involving repeated cracking and healing cycles. Their findings led to the conclusion that the inclusion of crystalline admixtures in the concrete samples had the potential to enhance the concrete's long-term self-healing ability under repeated cracking and healing cycles. Kannikachalam et al. [25] performed the fatigue testing on UHPC beams to evaluate the effectiveness of self-healing. After the samples were pre-cracked and subjected to up to 700,000 cycles at between 10 and

80% of the pre-crack load, the samples were repeatedly loaded for 100,000 cycles after a healing period of 1, 3, or 6 months in water. Crack sealing was at least 80% after 1 month and as high as 100% after 3 months. UHPC's self-healing properties contributed to bending stiffness recovery by lowering the rate of crack opening by up to 18 times throughout the fatigue cycles.

Studies above have examined the ability of suitable self-healing materials to maintain high levels of self-healing even after multiple cycles of cracking and healing. The authors' earlier review paper comprehensively addressed the influence of exposure to various environments on the self-healing performance of UHPC [18]. Nevertheless, the study on the impact of aggressive environments on the repeatability of self-healing performance of UHPC has been largely overlooked. In reality, understanding the implications of the external environment on self-healing efficacy is crucial for developing robust self-healing materials and ensuring their long-term reliability in practical applications.

By addressing this research gap, this study aims to shed light on the capacity of UHPC to maintain its self-healing capabilities in the face of repeated damage and aggressive conditions. To accomplish this, UHPC specimens with a double-edged wedge splitting geometry were utilized, incorporating a commercial crystalline admixture (Penetron Admix®). This particular geometry allows for the convenient assessment of the relationship between tensile stress and crack opening in fibre-reinforced cementitious composites [26]. To evaluate the healing capacity of the UHPC, samples were pre-cracked up to 0.3 mm cracking opening displacement (COD), as measured in the loading stage. This value of the COD was selected, also based on previous investigations [27], to have upon unloading a residual crack width in the rage of 0.05–0.1 mm, as

it will be hereafter detailed, deemed as representative of serviceability limit state situations for the investigated category of materials. The pre-cracked specimens were then subjected to three distinct water immersion exposure environments: tap water, salt water, and geothermal water. The closure of cracks over various curing periods was meticulously documented using optical microscopy. Additionally, tailored tests such as ultrasonic pulse velocity (UPV) measurements and double edge wedge splitting tensile tests, as already employed for pre-cracking, were conducted to quantify the recovery of mechanical properties. Through an exhaustive experimental investigation, this study seeks to offer a thorough insight into the aforementioned relationship within the examined materials. It specifically emphasizes their capacity to sustain mechanical properties when exposed to challenging conditions such as geothermal water and saltwater. This resilience is attributed to their enduring and replicable self-healing capabilities over the long term.

2 Materials

The mixture proportion of UHPC investigated in this study is presented in Table 1. A water-to-binder ratio of 0.18 was used to achieve a highly compact and strong matrix. Additionally, 0.8% of the mass of cement crystalline admixture (Penetron Admix®) was included as a healing stimulant [23–25]. Table 2 presents the chemical components of the employed cement and slag. To obtain tensile hardening performance, 1.5% by volume of straight brass-plated steel fibres having a length of 20 mm and a diameter of 0.22 mm, were added. The fibres have a minimum tensile strength of 2400 MPa. The detailed procedure for preparing the UHPC is referenced in the authors' previous publication [28].

Table 1 Mixture proportions of UHPC

Constituents (kg/m^3)						
CEMI 52.5 R	Slag	Water	Steel fibers	Sand 0–2 mm	Superplasticizer (SP)	Crystalline Admixture(CA)
600	500	200	120	982	33	4.8

CEM I according to European classification is a Portland cement with > 95% clinker

Table 2 Composition of cement and slag

Oxide (wt%)	CaO	SiO$_2$	Al$_2$O$_3$	MgO	SO$_3$	Fe$_2$O$_3$	TiO$_2$	Mn$_2$O$_3$/MnO	K$_2$O	Na$_2$O	Other	LOI
Cement	59.7	19.5	4.9	3.3	3.4	3.5	0.2	0.1	0.8	0.2	0.4	2.5
Slag	39.2	38.9	10.2	6.4	1.3	0.4	0.6	0.3	0.5	0.8	0.3	1.2
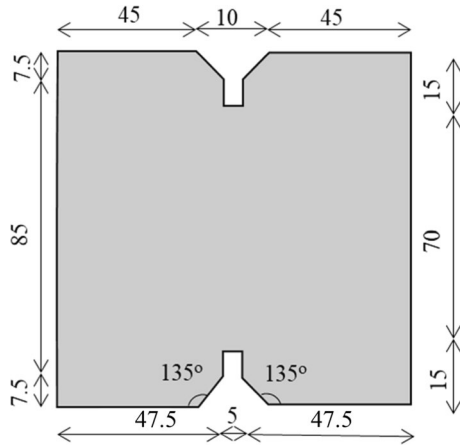
Fig. 1 Geometry of DEWS sample(unit:mm)

3 Experimental procedures

3.1 Preparation of the pre-cracked samples

Large slabs of UHPC were cast and subsequently cut into beams with $500 \times 100 \times 50$ mm [7, 28]. These beams were then stored at a controlled temperature of 20 °C and humidity of 90% for a maximum duration of 1 year to minimize the impact of delayed hydration on the self-healing properties. To assess the relationship between tensile stress and crack opening displacement (COD), the beam samples were further processed into double edge wedge splitting (DEWS) samples, as depicted in Fig. 1. Previous studies have confirmed that this testing methodology is particularly effective for straightforward identification of UHPC tensile constitutive behaviour [24, 26, 28].

The DEWS samples underwent a pre-cracking phase under displacement-controlled Instron machine, with a loading rate of 0.005 mm/s. The crack opening displacement (COD) at the midsection of both sample surfaces was recorded using linear variable differential transformers (LVDTs), as illustrated in Fig. 2. Once the average COD measured by the LVDTs reached 0.30 mm, unloading tests were
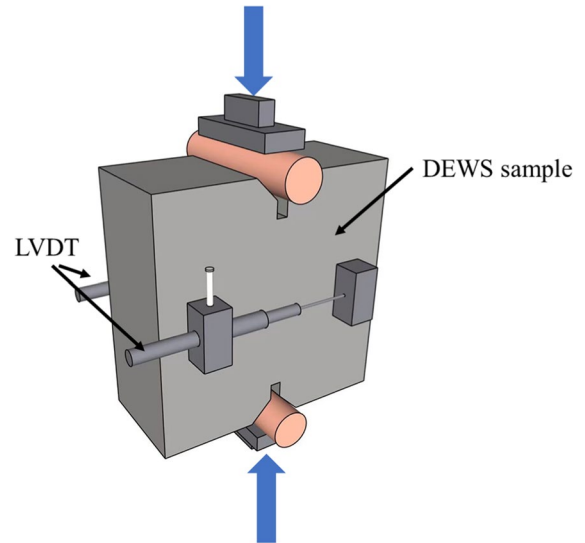
Fig. 2 Set-up of pre cracking test

conducted at the same loading speed, allowing for the acquisition of the complete loading and unloading curves for each sample.

After the pre-cracking tests, the cracked samples were immersed in three different water environments: tap water, salt water, and geothermal water. The tap water used was sourced from the municipal water supply network of Milan. The salt water was prepared with a concentration of 3.3% of sodium chloride As for the geothermal water, it was obtained from a geothermal power plant located in Chiudino, Tuscany [29]. Table 3 provides the chemical composition of the geothermal water, which exhibits a notably high content of sulphates and chlorides.

3.2 Re-cracking test

After precracking stage described above and immersion in the relevant environments, the DEWS samples were then subjected to cracking-healing cycles protocols according to the following procedure: after 1 month of exposure, the first re-cracking was

Table 3 Composition of the geothermal water (in ppm)

Compositions	Al	Ca	Fe	K	Mg	Na	S	Si	SO_4^{2-}	Cl
Quantity	0.2	4	0.13	19.8	0.3	1243	1523	0.3	2678	441
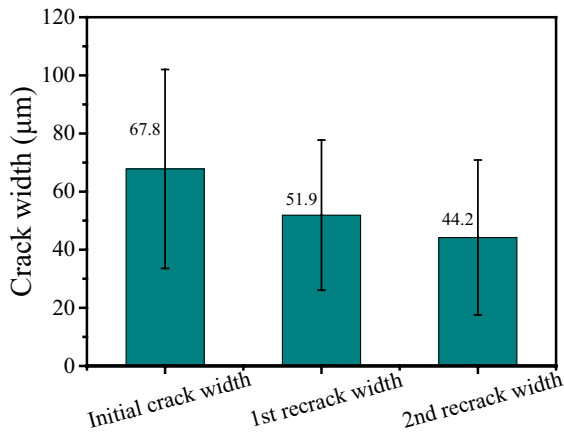
Fig. 3 Distribution of crack width (The error bar is standard deviation)

Fig. 4 Scheme of cracking-healing cycles

performed to keep 0.3 mm COD. Subsequently, after additional 2 months of exposure, the second re-cracking was conducted up to a 0.3 mm target COD under loading. It is worth remarking that in this stage the crack opening was measured starting from the existing state of the specimen. Lastly, after completion of three further months of exposure, a final splitting test was executed until sample failure. For each exposure condition three nominally identical replicas were tested.

Figure 3 shows the distributions of crack width for the samples after initial cracking, 1st and 2nd re-cracking. The average crack widths of UHPC samples are 67.8 µm, 51.9 µm and 44.2 µm after initial cracking, 1st and 2nd re-cracking respectively. The inherent variability in material properties and fiber dispersion, which could potentially influence the unloading response, may be invoked to rationalize the observed dispersion in crack width at the conclusion of unloading. In addition, reference samples without crack/healing cycles were set up for each stage. The reference samples were exposed continuously for 1 month, 3 months and 6 months after pre-cracking, and then subjected to splitting tests until failure. Also in this case for each exposure condition and duration three nominally identical specimens were tested.
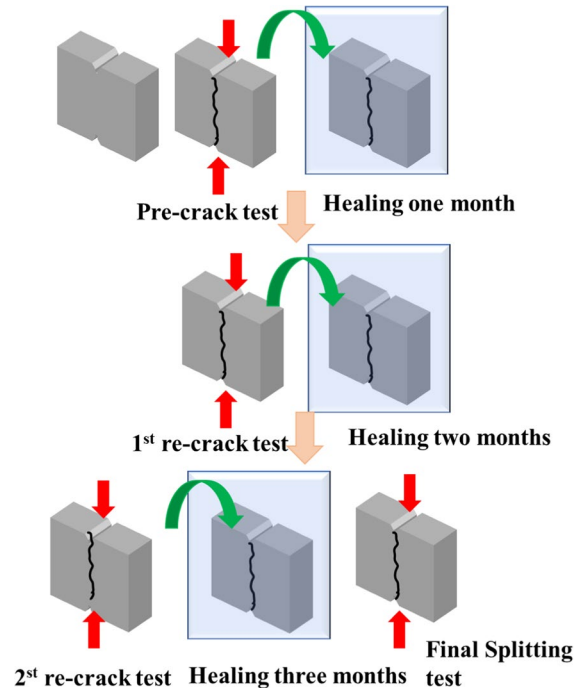
Figure 4 presents the crack/healing cycles scheme:

1. pre-cracked samples→immersion in tap/salt/geothermal water for 1–3–6 months without 1st and 2nd re-cracking and healing cycles→final splitting test;

2. sample with 1st and 2nd re-cracking and healing cycles: pre-cracked samples→healing in tap/salt/geothermal water for 1 month→1st re-cracking and healing cycle→healing in tap/salt/geothermal water for 2 months→2nd re-cracking and healing cycle→healing in tap/salt/geothermal water for 3 months→final splitting test.

3.3 Microscopic techniques for the evaluation of crack closure

The crack width in the samples was recorded at different curing times using a digital optical microscope and the DinoLite Capture software. To capture the complete crack, multiple photographs of each crack were merged in Phothoshop®, as shown in Fig. 5. The area (A_{area}) and length (l_{length}) of the cracks were then determined using the mathematical and statistical tools available in Phothoshop®. The average crack width was obtained by dividing A_{area} by l_{length}. The crack closure capacity was assessed by calculating the crack self-sealing index (ICS) according to Eq. (1).

$$\text{Index of crack self sealing} = \frac{W_{initial} - W_{aftersealing}}{W_{initial}} \tag{1}$$

where $w_{initial}$ represents initial crack width; $w_{after\ sealing}$ denotes the crack width after the specimen had been immersed in various water environments for the designated duration.

3.4 Ultrasonic pulse velocity test

The UPV test is a well-recognized and frequently employed method for assessing both the damage and self-healing capabilities of concrete [19, 30–32]. It involves the measurement of the velocity of the sound waves that propagate between an emitter and a receiver through the concrete. The velocity of these waves changes when passing through a discontinuity, typically a crack in concrete, as a function of the depth and width of the same crack. For the experiments conducted in this study, the distance between the transmitter and receiver was kept constant at 100 mm, equal to the specimen dimension, as illustrated in Fig. 6. The diameter of the transducer used for the test was 50 mm, and the frequency of the signal used was 50 kHz. The UPV tests were conducted on three types of samples: intact, pre-cracked, and sealed at different time periods. To calculate the wave velocity, the transmission time of the wave through the sample was recorded.

An index of velocity recovery (IVR) was proposed, as shown in Eq. (2), to compare the velocity of the sound waves through the intact, pre-cracked, and sealed
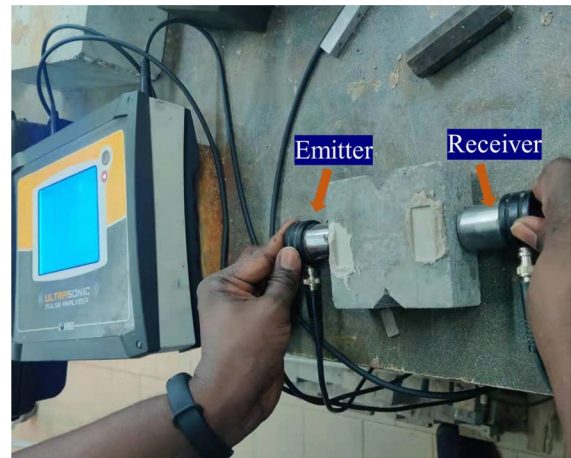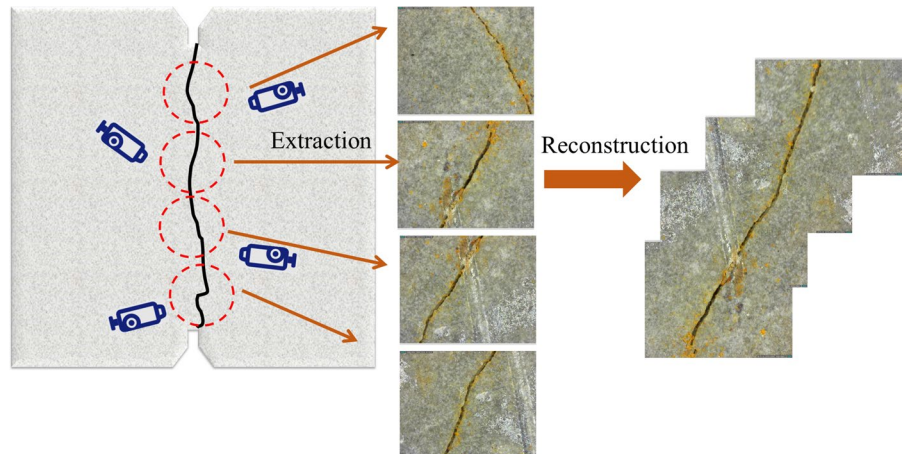

Fig. 6 Schematic diagram of UPV

Fig. 5 The process of crack extraction and reconstruction

samples. Hence, the extent of damage and the effectiveness of the self-healing process can be determined.

$$\text{IVR} = \frac{\text{UPV}_i}{\text{UPV}_{\text{intact}}} \quad (2)$$

where UPV_i represents the velocity of crack sample during i-th period; $\text{UPV}_{\text{intact}}$ denotes the velocity of the intact sample.

3.5 Index of stiffness recovery

The study focused on analysing the mechanical property recovery of DEWS samples through stress versus COD curves obtained from pre-cracking and post-healing re-cracking/failure tests. This was achieved by calculating the Index of Stiffness Recovery (ISR) and the equivalent post-healing re-cracking tensile stress σ_{eq}. The methodology employed for this analysis is succinctly delineated in Fig. 7, along with the corresponding Eq. (3). Equation (4) allows for the computation of the equivalent post-healing re-cracking tensile stress σ_{eq}, which is determined by dividing the work of fracture by the change in crack width [33], as also shown in Fig. 7.

$$\text{ISR} = \frac{K_{\text{loading,recracking}} - K_{\text{unloading,precracking}}}{K_{\text{loading,precracking}} - K_{\text{unloading,precracking}}} \quad (3)$$

where $K_{\text{unloading,precracking}}$ denotes initial unloading stiffness in precracking test; $K_{\text{loading,precracking}}$ represents initial loading stiffness in precracking test; $K_{\text{loading,recracking}}$ represents re-cracking stiffness in re-cracking test.

$$\sigma_{\text{eq}}[\text{MPa}] = W_F[\text{MPa mm}] \Big/ \left(w_{\text{max}} - w_{\text{min}}\right)[\text{mm}] \quad (4)$$

where w_{min} is the residual crack width of the pre crack; $w_{\text{max}(1st\ cycle)}$ is the sum of residual crack width of the pre crack and the maximum crack opening displacement under the peak stress of the 1st cycle; $w_{\text{max}(total)}$ is the aggregate of residual crack widths from the pre crack, residual crack widths from the 1st re-crack, and the maximum crack opening displacement observed during the peak stress of the 2nd cycle.

4 Results

4.1 Index of (ultrasonic pulse) velocity recovery (IVR)

IVR measurements were conducted on samples exposed to three different types of water: tap water, saltwater, and geothermal water, over varying time intervals. The IVR values, depicted in Fig. 8, demonstrate a consistent upward trend with prolonged exposure durations, indicating the occurrence of a self-healing mechanism within the cracks. Notably, the healing rate is most pronounced in tap water, while it is least effective in geothermal water. For reference, after 1 month, the IVR values are recorded as 0.98 for tap water, 0.963 for saltwater, and 0.932 for geothermal water. Subsequently, after 3 months, the IVR values exhibit marginal improvement, reaching 0.982, 0.972, and 0.938 for tap water, saltwater, and geothermal water, respectively. The IVR values of samples exposed to tap water during the first crack/healing cycle, closely resembled those of samples continuously soaked in tap water (Reference) for 3 months. Samples exposed to saltwater and geothermal water exhibit heightened IVR values after the first cracking/healing cycle. These values are not only comparable but, in some individual cases, surpass the values observed in samples consistently immersed in the same water conditions. Specifically, the average IVR values for saltwater and geothermal water
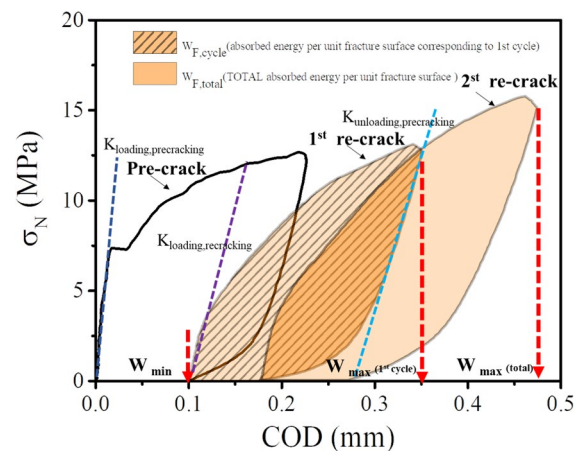

Fig. 7 Example of tensile stress (σ_N) versus COD curves. Methodology definition to obtain the absorbed energy per unit fracture surface (W_F), and $K_{\text{unloading,precracking}}$, $K_{\text{loading,precracking}}$ and $K_{\text{loading,recracking}}$

Fig. 8 Comparison of IVR (The reference samples are represented by solid lines, while the re-cracked samples are depicted with dashed lines.)

4.2 Index of crack sealing (ICS)
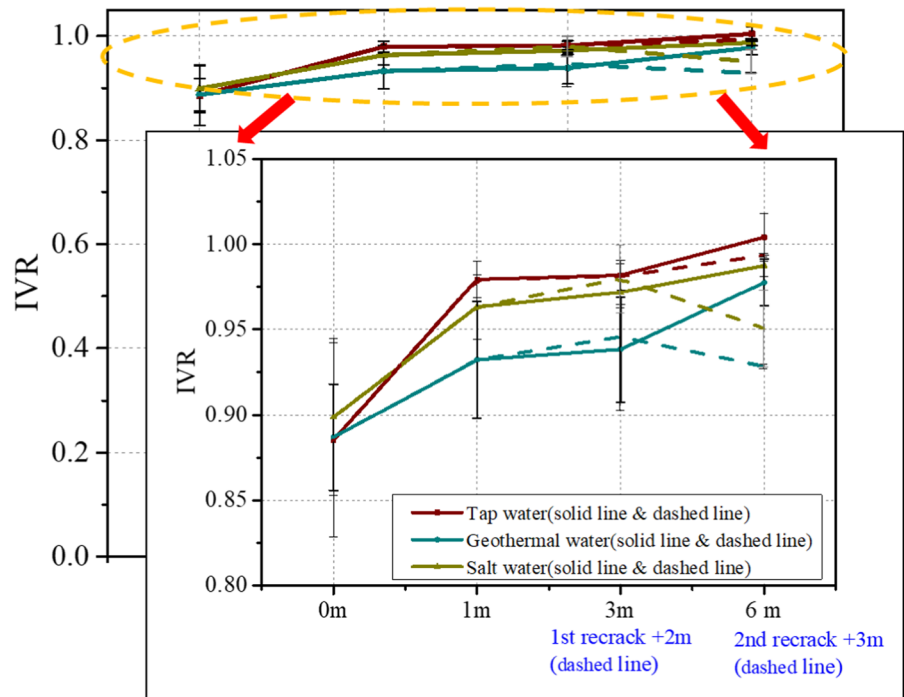
are measured at 0.98 and 0.946, respectively. The close proximity of these values suggests that the first re-cracking does not adversely affect the self-healing performance. This resilience is attributed to the formation of new reactive products, facilitated by the exposure to the healing environment, which incorporates fresh, unreacted material into the reopened cracks.

Nonetheless, as the samples undergo the 2nd crack/healing cycle, it became evident that the velocity recovery significantly diminished in samples exposed to the water environment for a total of 3 months in comparison to those subjected to continuous immersion for a more extended period of 6 months. To illustrate, after 6 months of exposure to tap water, the IVR value for the samples is recorded at 1.004. Subsequently, in the 2nd cracking/healing cycle, the IVR value dropped to 0.993, which means that the ability to recover speed was weakened, but the value was still higher than 0.981 in the first cracking/healing cycle. For specimens exposed in aggressive environments after 2nd crack/healing cycle, the IVR value was at 98% of the first cycle and 97% in salt water and geothermal water, respectively, but the specimens still recovered more than 95% of the specimen's IVR value after initial cracking.

The typical change of crack width with exposure time in different water environment is shown in Fig. 9. Figure 10 further illustrates the variations in ICS over time for tap water, salt water, and geothermal water. The results demonstrate varying degrees of self-healing effects in all three environments as the exposure time increases. After 1 month, the ICS values for tap water, salt water, and geothermal water are 66.2%, 60.9%, and 44.7% respectively. This trend aligns with the findings of the UPV in first month.

Additionally, after the 1st crack/healing cycle, the ICS values reach 76.5% in tap water, 71.7% in saltwater, and 67.4% in geothermal water. Notably, these figures exceed the ICS values observed in samples consistently exposed to tap water and geothermal water over a 3-month period. This phenomenon unfolds due to the reopening of partially sealed cracks, allowing for deeper water penetration into the crack inside. Subsequently, this triggers an extensive hydration reaction, facilitating the closure of these cracks.

It is worth noting, however, that the continued effectiveness of this cyclical model in enhancing ICS is less effective. After undergoing the 2nd crack/

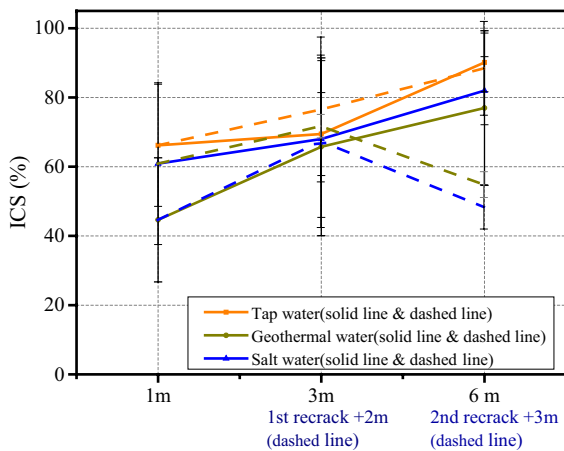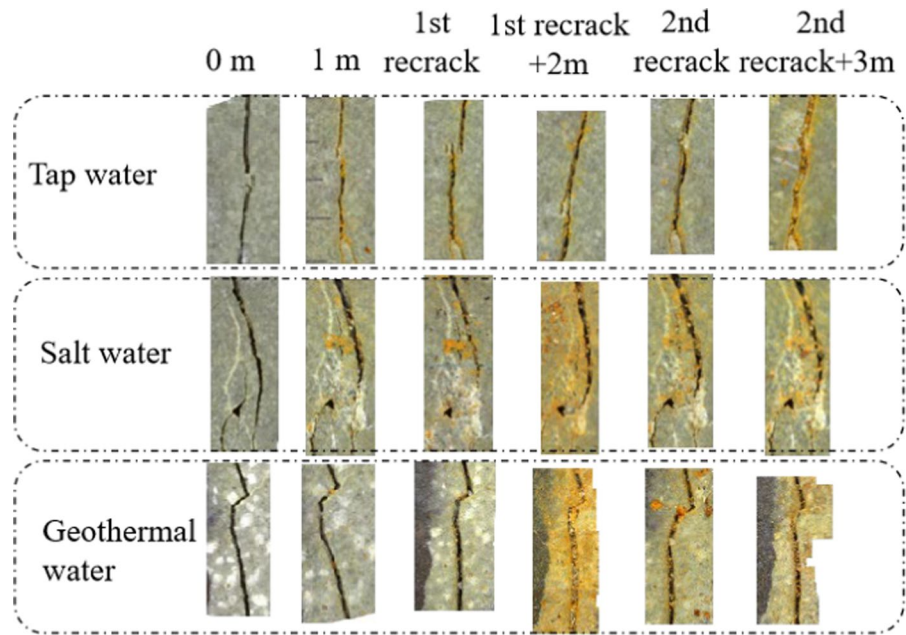**Fig. 9** Variation of crack width in different environments and times

Fig. 10 Comparison of ICS (The error bar is standard deviation—The reference samples are represented by solid lines, while the recracked samples are depicted with dashed lines.)

healing cycle, the ICS significantly decreases compared to samples exposed to water continuously for 6 months. The ICS values register at 88.4%, 54.9%, and 48.4% for exposure to tap water, saline water, and geothermal water, respectively. These values are notably inferior to those exhibited by samples subjected to continuous water exposure for the aforementioned 6-month duration, which record ICS values of 90.1%, 82%, and 76.9%, respectively. The ICS values

for exposure to salt water and geothermal water, are lower than those for the 1st cycle. Several factors are likely to contribute to this outcome. Firstly, a second cracking event can cause further damage to the sample and widen the fracture, making it more challenging to heal. Secondly, increased crack opening leads to heightened penetration of aggressive ions, which hinders the crystallization of self-healing products [27].

4.3 ISR

ISR calculations were performed for each tested sample under different environments and time intervals using Eq. (3) and Fig. 7. Figure 11 illustrates that, after 1 month, varying degrees of stiffness recovery are observed in all samples. The ISR values are calculated as 25.8%, 20.1%, and 15.6% for tap water, salt water, and geothermal water, respectively. This indicates that the cracks are not only sealed but also healed. The cracked UHPC exhibited the ability to restore its mechanical properties due to the self-healing effect.

After undergoing 3 months of continuous water exposure, the ISR values exhibit notable improvements, with values reaching 32.3% for tap water, 30% for saltwater, and 24.9% for geothermal water. Notably, the samples subjected to the 1st cycle display
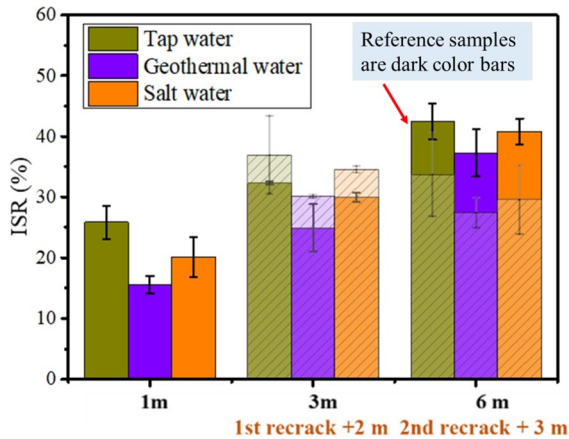
Fig. 11 Comparison of ISR values. (re-cracked samples are transparent bars)

Fig. 12 Comparison of equivalent tensile stress σ_{eq}

higher ISR: 36.9% for tap water, 34.5% for salt water, and 30.2% for geothermal water. This observed trend is consistent with the findings regarding UPV and ICS. The prolonged exposure of the crack to water leads to increased hydration reactions, and re-opening the cracks allows more Ca^{2+} to be released from the cement to penetrate inside the cracks, where they are more involved in the healing reaction thus promoting crack closure.

However, it is crucial to note that, following the 2nd cycle, ISR values exhibit a significant decline when compared to the values obtained after 6 months of continuous water exposure. The ISR values decreased to 33.7% for tap water, 29.5% for saltwater, and 27.4% for geothermal water after 2nd cycle. These figures align closely with those observed after just 3 months of continuous water immersion. Repeated loading exacerbates the damage and, which, with the progressive consumption of the available reactive particles in the UHPC sample, contribute to decrease the level of self-healing and stiffness recovery.

Nonetheless, it is worth highlighting that, despite experiencing multi cracking damage, UHPC demonstrated a notable degree of toughness recovery following a self-healing period, even when subjected to harsh environmental conditions. This observation underscores the enduring effectiveness of the self-healing mechanism.

Furthermore, Fig. 12 presents the calculations for equivalent tensile stress σ_{eq}. After the 1st recracking,
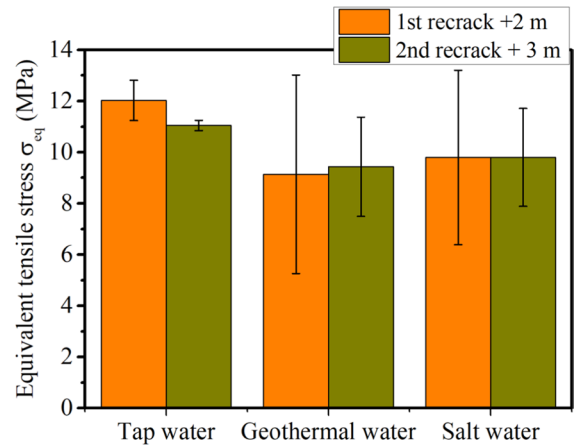
σ_{eq} exhibit the highest value in tap water at 12 MPa. It is closely followed by saltwater, reaching at 9.8 MPa, and geothermal water, which has the lowest σ_{eq} value of 9.1 MPa. Following the 2nd cracking, these values are 11, 9.8, and 9.4 MPa, respectively, for the aforementioned water environments. The calculated values in equivalent tensile stress, and their trends for the different loading and healing scenarios, provide further confirmation to the evidence, put forward e.g. in [34], that the mechanical crack healing phenomena also occurs at the fibre-matrix interface level, affecting the recovery/persistence of the fibre-matrix bondand hence directly resulting into the calculated recovery of the mechanical capacity [34].

4.4 Relationship between the different self-healing indicators

Figure 13 plots the relationships between the indicators. Their Pearson correlation coefficients (r) are more than 0.5, showing positive correlation. This further confirms that the mechanical properties and the level of self-healing recovery are highly correlated. ICS is from a microscopic observation of the crack surface, while IVR is from a qualitative measure of internal crack closure. Both indicators show a very high correlation coefficient ($r=0.882$), suggesting that crack healing exists not only on the crack surface but also within the crack. This promotes further recovery of the mechanical properties. It is worth noting that an ISR greater than 35% requires significant crack healing (ICS greater than 70%).

Fig. 13 The relationship between the evaluation indicators of self-healing effect

(a) IVR VS ICS

(b) IVR VS ISR

(c) ISR VS ICS

(d) equivalent tensile stress σ_{eq} VS ISR
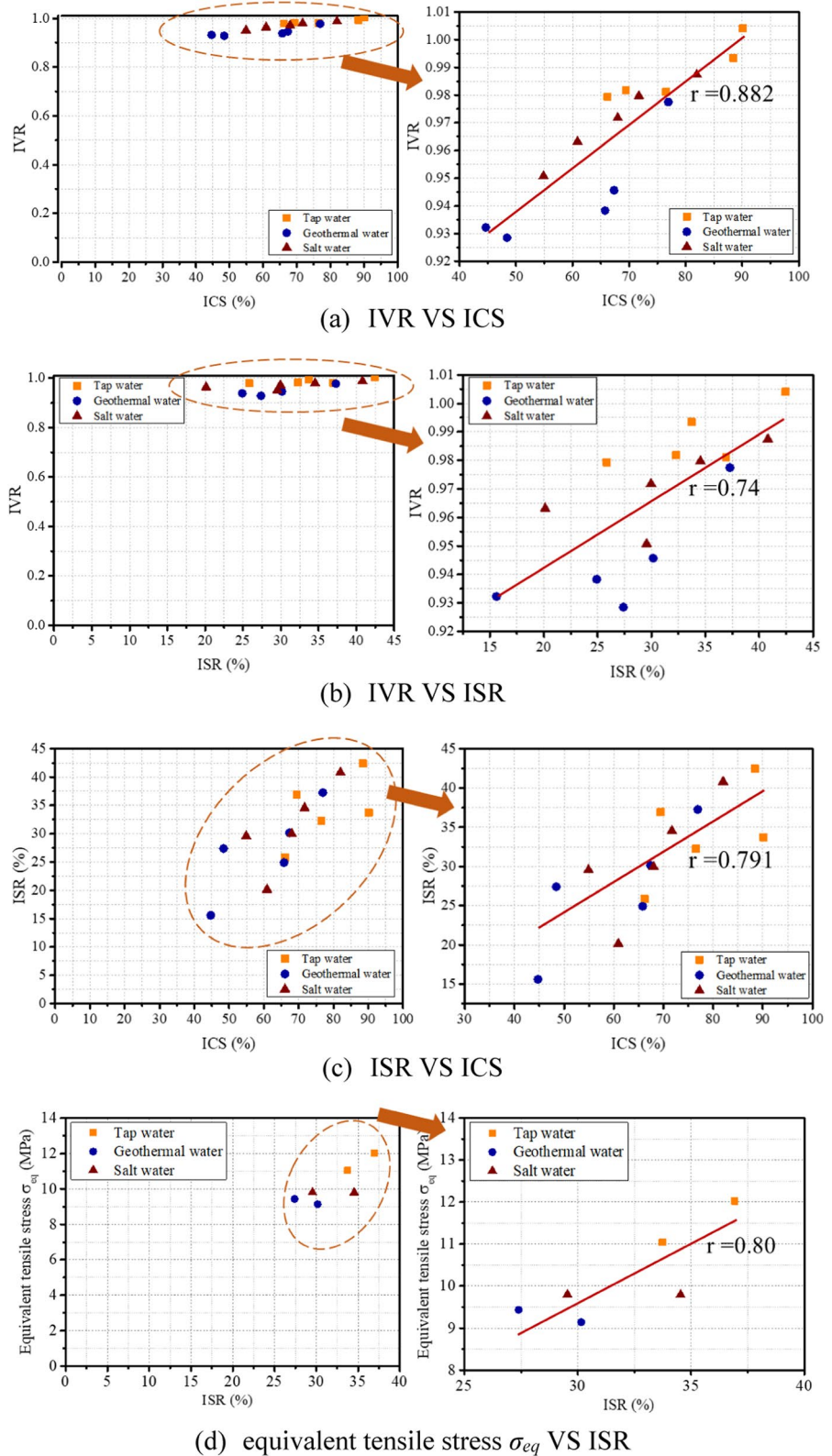
In addition, Fig. 13d shows that the equivalent tensile stress σ_{eq} and ISR also exhibit a strong correlation coefficient ($r = 0.80$). The increased level of self-healing also enhances the properties of the interface between the fibres and the matrix, allowing further recovery of the overall mechanical properties obtained.

5 Conclusions

This study conducted an investigation involving cracked UHPC samples exposed to diverse environments such as tap water, saltwater, and geothermal water, with the aim of evaluating the repeatability and stability of their healing capabilities under a series of subsequent cracking and healing cycles. The samples were subsequently exposed to different conditions for periods of 1, 3, and 6 months. After each of these intervals, the samples were re-cracked and then subjected to same exposure conditions for an extra 2 or 3 months, allowing for the repetition of the cracking and healing process. The average crack widths of UHPC samples were 67.8 μm, 51.9 μm and 44.2 μm after initial cracking, 1st and 2nd recracking. The healing effectiveness was evaluated by means of visual analysis of crack closure as well as through the recovery of physical (Ultrasonic Pulse Velocity) and mechanical (stiffness and equivalent post-cracking stress) performance.

Overall, the study has revealed a self-healing which improved after the 1st crack/self-healing cycle, likely because of the possibility of exposing to the healing environment new unreacted fresh material inside the cracks, and steadily declined after the 2nd cycle, likely due to progressive consumption of the available reactive material and likewise progressive closure and reduced further residual opening of the new cracks. Nonetheless, even after having experienced two cycles of healing/cracking, UHPC samples still maintained good levels of self-healing and mechanical property recovery regardless of the type of water they were exposed to. In detail:

1. The results related to recovery of ultrasonic pulse speed exhibit an incremental trend with prolonged exposure time, signifying the closure of cracks. Notably, healing is most pronounced in tap water and least effective in geothermal water. Furthermore, an increase in the UPV is evident following the 1st crack/healing cycle. However, velocity recovery experiences a significant decline when the samples undergo the 2nd cracking/healing cycle.

2. A comparison of the Index of Crack Sealing values reveals a consistent increase in ICS with prolonged exposure time across all three environments. Following the 1st cracking/healing cycle, ICS values stand at 76.5% in tap water, 71.7% in saltwater, and 67.4% in geothermal water. These values exceed those observed in samples continuously exposed to the same water environment for 3 months. This phenomenon occurs as partially sealed cracks reopen, facilitating deeper water penetration and triggering extensive hydration reactions that lead to crack closure. After the 2nd crack/healing cycle, a significant decrease in ICS is evident, with values of 88.4%, 54.9%, and 48.4% for exposure to tap water, saltwater, and geothermal water, respectively.

3. Different levels of stiffness recovery have been observed in all samples. After 1 month of exposure to tap water, saltwater, and geothermal water, the ISR values are 25.8%, 20.1%, and 15.6%, respectively, indicating that cracked UHPC has the capability to restore its mechanical properties. Notably, samples after the 1st cycle exhibit higher ISR values: 36.9% for tap water, 34.5% for saltwater, and 30.2% for geothermal water. However, after the 2nd cycle, ISR values decline to 33.7% for tap water, 29.5% for saltwater, and 27.4% for geothermal water. This decrease is attributed to repeated loading, which increases damage and reduces the number of reactive particles in the UHPC samples, thereby diminishing both self-healing and stiffness recovery capabilities.

4. Despite enduring multiple crack damages, UHPC samples continue to demonstrate a noteworthy degree of toughness recovery, attributed to the self-healing effect also at the level of fibre-matrix interface. This observation underscores the enduring efficacy of the self-healing mechanism, even in aggressive environmental conditions.

ReSHEALience project (Rethinking coastal defense and Green-energy Service infrastructures through enHancEd-durAbiLity high-performance cement-based materials) which has received funding from the European Union's Horizon 2020 research and innovation program under grant agreement No 760824. The help of Mr. Antonio Cocco, Mr. Paolo Broglia and Mr. Giuseppe Pappadà (Laboratory for Testing Materials, Buildings and Structures, Politecnico di Milano) in cutting the specimens for the experimental program and providing organizational support for its execution is gratefully acknowledged. Bin Xi also acknowledges the financial support of the China Scholarship Council (CSC) under the grant No.202008440524 for PhD study in Structural Geotechnical and Earthquake Engineering at Politecnico di Milano.

Declarations

Conflict of interest   The authors declare that they have no known competing financial interests or personal relationships that could have appeared to influence the work reported in this paper.

References

1. de Brito J, Kurda R (2021) The past and future of sustainable concrete: a critical review and new strategies on cement-based materials. J Clean Prod 281:123558. https://doi.org/10.1016/j.jclepro.2020.123558

2. Zhu Y, Hussein H, Kumar A, Chen G (2021) A review: material and structural properties of UHPC at elevated temperatures or fire conditions. Cem Concr Compos 123:104212. https://doi.org/10.1016/j.cemconcomp.2021.104212

3. Beushausen H, Torrent R, Alexander MG (2019) Performance-based approaches for concrete durability: state of the art and future research needs. Cem Concr Res 119:11–20. https://doi.org/10.1016/j.cemconres.2019.01.003

4. De Belie N, Gruyaert E, Al-Tabbaa A et al (2018) A review of self-healing concrete for damage management of structures. Adv Mater Interfaces 5:1800074. https://doi.org/10.1002/admi.201800074

5. Du J, Meng W, Khayat KH et al (2021) New development of ultra-high-performance concrete (UHPC). Compos Part B Eng 224:109220. https://doi.org/10.1016/j.compositesb.2021.109220

6. Bajaber MA, Hakeem IY (2021) UHPC evolution, development, and utilization in construction: a review. J Mater Res Technol 10:1058–1074. https://doi.org/10.1016/j.jmrt.2020.12.051

7. Cuenca E, D'Ambrosio L, Lizunov D et al (2021) Mechanical properties and self-healing capacity of ultra high performance fibre reinforced concrete with alumina nano-fibres: tailoring ultra high durability concrete for aggressive exposure scenarios. Cem Concr Compos 118:103956. https://doi.org/10.1016/j.cemconcomp.2021.103956

8. Xi B, Huang Z, Al-Obaidi S, Ferrara L (2023) Predicting ultra high-performance concrete self-healing performance using hybrid models based on metaheuristic optimization techniques. Constr Build Mater 381:131261. https://doi.org/10.1016/j.conbuildmat.2023.131261

9. ACI Committee 239 (2018) Ultra-High-performance concrete: an emerging technology report (ACI 239R–18). Am Concr Inst

10. Vinet L, Zhedanov A (2011) A 'missing' family of classical orthogonal polynomials. J Phys A Math Theor 44:085201. https://doi.org/10.1088/1751-8113/44/8/085201

11. Larsen IL, Thorstensen RT (2020) The influence of steel fibres on compressive and tensile strength of ultra high performance concrete: a review. Constr Build Mater 256:119459. https://doi.org/10.1016/j.conbuildmat.2020.119459

12. Teng L, Huang H, Khayat KH, Gao X (2022) Simplified analytical model to assess key factors influenced by fiber alignment and their effect on tensile performance of UHPC. Cem Concr Compos 127:104395. https://doi.org/10.1016/j.cemconcomp.2021.104395

13. Graybeal B, Brühwiler E, Kim B-S et al (2020) International perspective on UHPC in bridge engineering. J Bridg Eng. https://doi.org/10.1061/(ASCE)BE.1943-5592.0001630

14. Barutha P, Nahvi A, Cai B et al (2019) Evaluating commercial feasibility of a new tall wind tower design concept using a stochastic levelized cost of energy model. J Clean Prod 240:118001. https://doi.org/10.1016/j.jclepro.2019.118001

15. Amran M, Huang SS, Onaizi AM et al (2022) (2022) Recent trends in ultra-high performance concrete (UHPC): current status, challenges, and future prospects. Constr Build Mater 352:129029

16. Cappellesso V, di Summa D, Pourhaji P et al (2023) A review of the efficiency of self-healing concrete technologies for durable and sustainable concrete under realistic conditions. Int Mater Rev. https://doi.org/10.1080/09506608.2022.2145747

17. Kannikachalam NP, Marin Peralta PS, Snoeck D et al (2023) Assessment of impact resistance recovery in Ultra High-performance concrete through stimulated autogenous self-healing in various healing environments. Cem

Concr Compos 143:105239. https://doi.org/10.1016/j.cemconcomp.2023.105239

18. Xi B, Al-Obaidi S, Ferrara L (2023) Effect of different environments on the self-healing performance of ultra high-performance concrete—a systematic literature review. Constr Build Mater 374:130946. https://doi.org/10.1016/j.conbuildmat.2023.130946

19. Davolio M, Al-Obaidi S, Altomare MY et al (2023) A methodology to assess the evolution of mechanical performance of UHPC as affected by autogenous healing under sustained loadings and aggressive exposure conditions. Cem Concr Compos 139:105058. https://doi.org/10.1016/j.cemconcomp.2023.105058

20. Hilloulin B, Van Tittelboom K, Gruyaert E et al (2015) Design of polymeric capsules for self-healing concrete. Cem Concr Compos 55:298–307. https://doi.org/10.1016/j.cemconcomp.2014.09.022

21. Wang Y-S, Lee H-S, Lin R-S, Wang X-Y (2022) Effect of silicate-modified calcium oxide-based expansive agent on engineering properties and self-healing of ultra-high-strength concrete. J Build Eng 50:104230. https://doi.org/10.1016/j.jobe.2022.104230

22. Zhang D, Shahin MA, Yang Y et al (2022) Effect of microbially induced calcite precipitation treatment on the bonding properties of steel fiber in ultra-high performance concrete. J Build Eng 50:104132. https://doi.org/10.1016/j.jobe.2022.104132

23. Snoeck D, De Belie N (2016) Repeated autogenous healing in strain-hardening cementitious composites by using superabsorbent polymers. J Mater Civ Eng. https://doi.org/10.1061/(ASCE)MT.1943-5533.0001360

24. Cuenca E, Tejedor A, Ferrara L (2018) A methodology to assess crack-sealing effectiveness of crystalline admixtures under repeated cracking-healing cycles. Constr Build Mater 179:619–632. https://doi.org/10.1016/j.conbuildmat.2018.05.261

25. Niranjan Prabhu K, Vela DAC, Pacheco YGO, et al (2022) Fatigue behavior and effect of stimulated autogenous self-healing in Ultra High-Performance Concrete. In: fib symposium

26. di Prisco M, Ferrara L, Lamperti MGL (2013) Double edge wedge splitting (DEWS): an indirect tension test to identify post-cracking behaviour of fibre reinforced cementitious composites. Mater Struct 46:1893–1918. https://doi.org/10.1617/s11527-013-0028-2

27. Bin X, Zhewen H, Al-Obaidi S, Ferrara L (2022) Healing capacity of Ultra High Performance Concrete under sustained through crack tensile stresses and aggressive environments. Cem. Concr. Compos. Accepted

28. Cuenca E, Postolachi V, Ferrara L (2023) Cellulose nanofibers to improve the mechanical and durability performance of self-healing ultra-high performance concretes exposed to aggressive waters. Constr Build Mater 374:130785. https://doi.org/10.1016/j.conbuildmat.2023.130785

29. Al-Obaidi S, Bamonte P, Animato F et al (2021) Innovative design concept of cooling water tanks/basins in geothermal power plants using ultra-high-performance fiber-reinforced concrete with enhanced durability. Sustainability 13:9826. https://doi.org/10.3390/su13179826

30. Komloš K, Popovics S, Nürnbergerová T et al (1996) Ultrasonic pulse velocity test of concrete properties as specified in various standards. Cem Concr Compos. https://doi.org/10.1016/0958-9465(96)00026-1

31. Zhong W, Yao W (2008) Influence of damage degree on self-healing of concrete. Constr Build Mater. https://doi.org/10.1016/j.conbuildmat.2007.02.006

32. Naik T, Malhotra V, Popovics J (2003) The ultrasonic pulse velocity method. In: Handbook on nondestructive testing of concrete Second Edition. CRC Press, pp 8–1–8–19

33. Cuenca E, Ferrara L (2020) Fracture toughness parameters to assess crack healing capacity of fiber reinforced concrete under repeated cracking-healing cycles. Theor Appl Fract Mech 106:102468. https://doi.org/10.1016/j.tafmec.2019.102468

34. Alobaidi S, He S, Schlangen E, Ferrara L (2023) Effect of matrix self-healing on the bond-slip behavior of micro steel fibers in ultra high-performance concrete. Submitt Mater Struct 56:1–20. https://doi.org/10.1617/s11527-023-02250-5